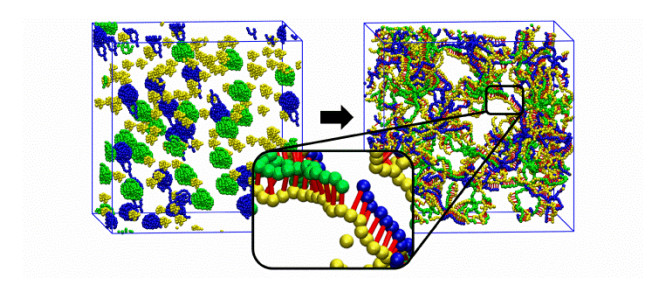
Computational study of DNA-crosslinked hydrogel formation for drug delivery applications

Kye Won Wang, ¹ Tania Betancourt, ^{2,3} Carol K. Hall^{1*}

- 1 Department of Chemical Engineering, North Carolina State University, Raleigh, NC, 27606
- 2 Department of Chemistry and Biochemistry, Texas State University, San Marcos, TX, 78666
- 3 Materials Science, Engineering, and Commercialization Program, Texas State University, San Marcos, TX, 78666

Corresponding author: hall@ncsu.edu



for Table of Contents use only

Computational study of DNA-crosslinked hydrogel formation for drug delivery applications

Abstract

In this paper, we present the results of discontinuous molecular dynamics (DMD) simulations aimed at understanding the formation of DNA-mediated hydrogels and assessing their drug loading ability. Poly(ethyleneglycol) (PEG) precursors of 4 and 6 arms that are covalently functionalized on all ends with oligonucleotides are crosslinked by a single oligonucleotide whose sequence is complementary to the oligonucleotide conjugated to the precursor. We show that the precursors with large molecular weight and many arms are advantageous in forming a three-dimensional percolated network. Analysis of the percolated networks shows that the pore diameter distribution becomes narrower as the precursor concentration, the number of arms, and the molecular weight increase. The pore throat diameter, the size of the largest molecule that can travel through the hydrogel networks without being trapped, is determined. The percolated network slows the movement of molecules inside the pores. Molecules larger than the pore throat diameter have more restrictions on their movement in the percolated network than those with smaller sizes.

Introduction

Hydrogels are three-dimensional networks of polymer chains¹ that are crosslinked via physical or chemical means². They are valued for their high water holding capacity (> 90 % water) ³⁻⁴, which gives them a flexibility that is similar to that of natural tissue and makes them biocompatible⁵⁻⁶. Hydrogels are used in a variety of applications including contact lenses⁷, wound healing dressings⁸⁻⁹, tissue engineering¹⁰⁻¹⁴, biosensors¹⁵, and drug delivery¹⁶⁻¹⁸.

The porous (or network) structure of the hydrogels makes them well suited for carrying small molecules such as therapeutics¹⁹ and biomolecules such as growth factors, hormones and protein therapeutics²⁰⁻²¹. The size of pores in a hydrogel controls the movement (diffusion) of entrapped small molecules, and has been the subject of experimental^{19, 22-25} and theoretical investigations²⁶⁻³⁰. In general, drugs whose diameter is smaller than the average pore size can quickly diffuse through the structure of the hydrogel, but drugs whose diameter is equal to or greater than the average pore size, are drastically slowed down^{26, 31}. The movement of a drug molecule through a hydrogel's non uniform pore structure is also related to the size of the "pore throat"^{25, 32}; that is the maximum size that a molecule can be and still travel in the hydrogel without limitations. In order to deliver drugs to a target site effectively, it is important to understand the relationship between the pore structure and drug size, the goal being to make hydrogel networks with appropriate pore size distributions and thus minimize premature drug loss.

Hydrogels prepared from poly(ethylene glycol) (PEG) have been used in a wide range of biomedical applications because PEG is a water soluble and non-toxic polymer ³³⁻³⁴. Among the various shapes of PEG hydrogels, those formed by multi-arm PEGs are useful when a highly

homogeneous internal structure is desired³⁵⁻⁴⁰. When the end of the PEG is modified with DNA and complementary DNA is added as a potential crosslinker, a hydrogel will form between these "precursors" as a result of the hybridization between DNA and its complement⁴¹⁻⁴². Hydrogels formed in this way have the advantage that all the components are biocompatible, that the crosslinking process is spontaneous, and that the crosslinks can be reversibly disrupted thermally and by competitive interaction with other complementary DNA strands⁴³. In instances where DNA aptamers are used, crosslinking can also be reversibly disrupted by the presence of the DNA aptamer.

We are engaged in a computational and experimental research project which aims to develop DNA-enabled micro- and nano-sized hydrogels formed by multi-armed PEG molecules. This paper is the second in a three-part series. The first paper describes the development of a coarse-grained (CG) model for simulation of DNA hybridization⁴⁴. In this, the second paper, we simulate the formation of the DNA-mediated hydrogel using the developed model, and assess the hydrogel's drug loading ability. In the third paper, we will simulate the degradation of the hydrogel when it encounters target molecules, thereby releasing previously-loaded drugs.

The goal of this research is to understand how the structure and concentration of the PEG precursors affect the formation and structure of hydrogels, and to predict the size of therapeutic molecules that can be entrapped and/or transported through them. The characteristics of the hydrogel structure (pore size) are determined by the precursor concentration, precursor structure, and degree of crosslinking¹⁹. The sizes of representative drugs are known to be the following: the hydrodynamic radius of rituximab is 54 Å, trastuzumab is 69 Å, ranibizumab is 28 Å, and aflibercept is 37 Å⁴⁵⁻⁴⁶. Rituximab is a chimeric monoclonal antibody used to treat several types

of cancer and autoimmune disorders. Trastuzumab is a monoclonal antibody that binds the HER2 receptor which is used for the treatment of breast cancer. Ranibizumab is a monoclonal antibody fragment that acts as an inhibitor of angiogenesis for the treatment of wet age-related macular degeneration. Aflibercept is a recombinant protein that also acts as an angiogenesis inhibitor. It is used for the treatment of macular degeneration and metastatic colon cancer. Here, we investigate (1) how the precursor concentration required to form a hydrogel depends on the number of arms of the precursors, (2) how the pore diameter depends on the precursor concentration and number of arms, and (3) how the pore structure affects the movement of molecules through the hydrogel. The benefit of this work is that we can find design parameters for preparation of DNA-crosslinked hydrogels with desired pore size so as to optimize drug retention and controlled release.

In this project, we conduct discontinuous molecular dynamics (DMD) simulations to model the formation and drug carrying ability of oligonucleotide-crosslinked hydrogels. The PEG precursors are covalently functionalized on their ends with oligonucleotides. Two different structures of oligonucleotide-functionalized PEG precursors are modeled in CG representation:

4-armed and 6-armed. The crosslinker is a CG oligonucleotide that is complementary to the oligonucleotide on the end of the PEG precursors. The precursors are hybridized with crosslinker oligonucleotides to form a hydrogel network. Water is treated implicitly. The precursors are randomly located in the simulation box initially, and spontaneous network formation is observed as the simulation proceeds. The percolation probabilities of the networks formed at various precursor concentrations are analyzed to determine the lowest precursor concentration required for hydrogel formation for each precursor shape and molecular weight. The pore size diameter distributions are calculated to learn how the shape, molecular weight, and concentration of

precursors influence the hydrogel porosity. In addition, based on analysis of the pore size distribution, we find the maximum size molecule that can travel through the hydrogel networks without being trapped, i.e. the pore throat diameter. Finally, to understand the effect of pore size distribution on the migration of molecules in the network, the mean square displacements (MSD) of different-sized spheres in the percolated networks are investigated.

Highlights of the results include the following. The network structures crosslinked by different types of precursors are simulated using the CG representation. The network formed by the 4- and 6-armed precursors exhibits a high degree of crosslinking for all precursor concentrations investigated. The 6-armed PEG requires lower precursor concentrations to form a hydrogel than the 4-armed PEG regardless of the precursor molecular weight. The pore size distribution becomes narrower with higher PEG molecular weight, number of arms, and concentration, and the average pore diameter decreases accordingly. All the percolated networks have heterogeneous porous structures, which limit the movement of the molecules within them. Molecules with a diameter equal to or smaller than the pore throat diameter cannot be confined inside the hydrogel matrix. Lastly, the diffusion coefficients of inserted spheres with various diameters are calculated from the MSD data, and the reduction in movement for each size sphere is estimated. The MSD results for small spheres inserted in the percolated networks demonstrate the potential of oligonucleotide-mediated hydrogels for use as drug delivery vehicles.

Model and method

Each CG ethylene oxide (EO) repeat unit (CH₂CH₂O) of PEG is represented by a single sphere that contains 2 carbons, 4 hydrogens, and 1 oxygen. PEG molecules are modeled as linear

chains of connected EOs. Two types of bonds are applied to maintain the connectivity and stiffness of CG PEG: covalent bonds and pseudobonds. The covalent bond is a real bond between adjacent CG EOs, and the pseudobond is an artificial bond between nonbonded CG EOs. Pseudobonds are imposed between a CG EO and the 2nd-nearest neighbor EO and between a CG EO and the 3rd-nearest neighbor EO. (The 2nd-nearest neighbor indicates EOs separated by one EO, and the 3rd-nearest neighbor indicates EOs separated by two EOs along the chain.)

The distance between the CG EOs fluctuate between maximum and minimum bond length values. When the bond length reaches the minimum or maximum distance, an infinitely-repulsive force is exerted so that they return to the proper bond length range⁴⁷⁻⁴⁸.

The values of the minimum and maximum distances between bonded CG EOs are determined by performing atomistic simulations. Simulations of united-atom PEG (Mw: 546.65 Da, number of repeat unit: 13) are performed with the GROMACS package to obtain the bond length distributions. Molecular topology information was obtained by using Automated Topology Builder (www.atb.com). The Lennard-Jones interaction parameters for the atoms in PEG are taken from Hezaveh's research data⁴⁹. Fifteen PEG chains were placed in a box of 100 Å × 100 Å, and 32548 water molecules were added to fill the box. Ninety six sodium cations and ninety six chlorine anions were inserted to mimic 160 mM salt conditions. The simulation was conducted for 20 ns at 310 K and 1.0 bar (NPT ensemble). The various bond length distributions were obtained by collecting the center of mass distance between the CG EOs. CG distributions for the covalent bond lengths, and for the bond and torsional angle pseudobond lengths similar to those in the atomistic simulation can be achieved by limiting the minimum and maximum distances to a proper range. The minimum real bond and pseudobond lengths were selected by finding the smallest distance at which the bond distribution function

reaches 30% of its maximum peak value, and the maximum real bond and pseudobond lengths were determined by finding the distance (larger than the maximum peak distance) where the bond distribution function reaches 30% of its maximum peak value. The so-determined CG bond lengths are as follows. The bond length between covalently-bonded CG EOs fluctuates with a minimum length of 2.985 Å and a maximum length of 3.685 Å. The pseudobond length for the bond angle has a minimum of 4.945 Å and a maximum of 6.935 Å, and the pseudobond length for the torsional angle has a minimum of 7.505 Å and a maximum of 10.025 Å.

The radial distribution functions (RDF) between two intermolecular CG EOs are obtained from center of mass data and used to define interaction parameters. The interaction between CG EO molecules are represented using the hard-sphere potential; this is because the EO-EO radial distribution function has no noticeable local maximum as would have resulted if there were molecular attractions. The hard sphere potential, u_{ij} , is

$$u_{ij}(r) = \begin{cases} & \infty & o < r \le \sigma_{ij} \\ & 0 & \sigma_{ij} < r \end{cases}$$

where r is the separation distance, and σ_{ij} is the sphere diameter between two EOs i and j. The hard-sphere diameter represents the minimum possible distance between a pair of non-bonded CG sites, and is determined by finding the shortest separation distance as reflected in the RDF between the CG sites. The hard sphere diameter (σ_{EO}) is determined to be 3.125 Å. Supplementary Figure 1 shows a comparison of the RDFs of atomistic and CG EO models.

Each nucleotide is modeled as a single CG interaction site to represent sugar, phosphate, and base. The model has four different types of nucleotides (adenine, thymine, cytosine, and guanine). According to the Watson-Crick base pairing rule, only adenine-thymine and cytosine-

guanine interactions need to be taken into account. The interactions between CG nucleotides are represented using the square-well potential; the model parameters were established in our previous research⁴⁴. The interactions between EO and nucleotides are considered as hard sphere for simplicity.

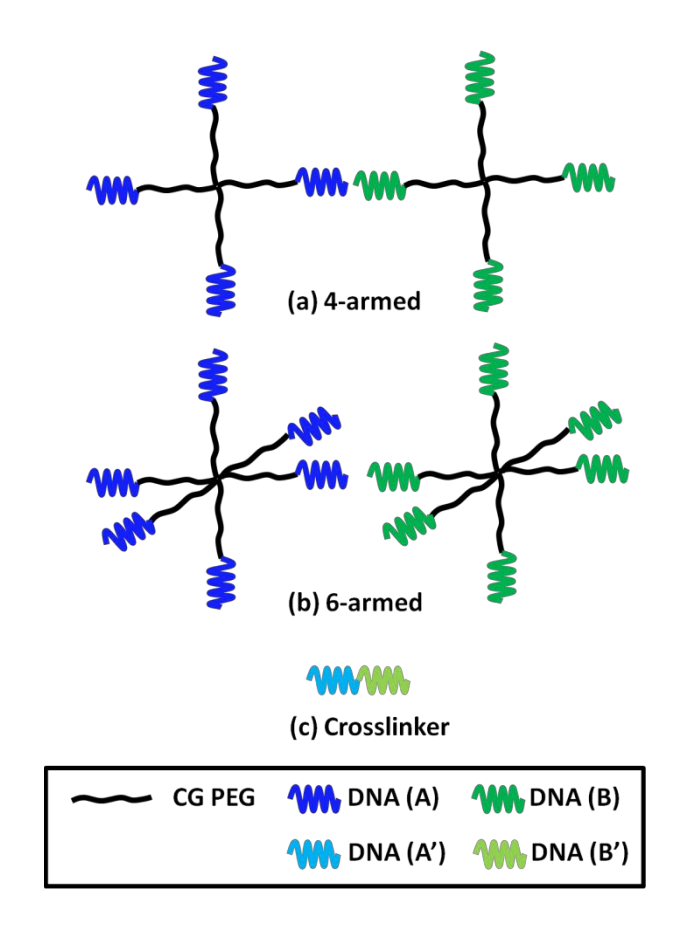


Figure 1. Schematic illustrations of (a) 4-armed, (b) 6-armed precursors, and (c) a crosslinker.

Figure 1 shows the structures of the hydrogel precursors and crosslinker oligonucleotides considered in the coarse grained representation. The hydrogel precursors contain two distinctive moieties, PEG (black) and oligonucleotide (blue and green). There are two different types of

PEGs; 4-armed, and 6-armed. The number of EO beads in the branch is determined by the molecular weight of PEG. PEGs with molecular weights of 2, 5, and 10 kDa were selected. Table 1 shows the number of EO repeat units on one branch for the different molecular weights and shapes.

	2 kDa	5 kDa	10 kDa
4-armed PEG	11	28	57
6-armed PEG	8	19	38

Table 1. Number of CG EOs in one branch for each shape and molecular weight PEG precursor.

The oligonucleotides are attached to the end of the PEG arms and act as crosslinking sites.

Two different oligonucleotide sequences are used: 5' GGACGGTGCGAGGCG 3' (DNA (A), blue in Figure 1) and GTGACTGGACCCCC (DNA (B), green in Figure 1). These sequences are chosen because their melting temperatures are higher than body temperature. Thus, the given oligonucleotides could be used for crosslinking since the hybridized state between those oligonucleotides and their complements would be maintained in the human body. The PEG precursor functionalized by the oligonucleotide sequence GGACGGTGCGAGGCG is called Precursor A, and the PEG precursor functionalized by GTGACTGGACCCCC is called Precursor B. The sequence of the crosslinker oligonucleotide is 5'

CCTGCCACGCTCCGCCACTGACCTGGGGG 3', which is the concatenation of the complementary oligonucleotides of the two oligonucleotides described above (schematically represented as DNA (A') and DNA (B') in Figure 1). Base pairings between those oligonucleotides are the driving force for crosslinking. The crosslinking is formed by connecting

Precursors A and B via the crosslinker.

Discontinuous molecular dynamics (DMD) simulations is used to simulate the formation of hydrogels and the movement of spheres (model therapeutics) through the hydrogel. DMD is a fast alternative to traditional MD that is applicable to systems of molecules interacting via discontinuous potentials. Because the discontinuous potential forces on the particles are exerted only when the particles collide, the computational costs of DMD are lower than in traditional MD, and this allows the study of longer time scales and larger systems. The DMD algorithm calculates the collision times among all the pair-wise collisions and advances the time to the point that the soonest collision occurs. Unlike conventional MD, which uses a constant time step, the time step of DMD is different in every calculation, so that the progress of the simulation is expressed in terms of the number of collisions.

The details of the CG DMD simulations of the hydrogel formation are as follows. Initially, 20 Precursor A and 20 Precursor B chains are randomly placed in a box. The numbers of crosslinker oligonucleotides in the box are set to be 100 and 140, respectively, for 4-armed and 6-armed precursors . The actual number of crosslinkers is set to be one more than the number required for complete crosslinking between precursor A and B because this condition promoted a high rate of polymerization in past experiments by one of us. The lengths of each side of the box were selected to mimic precursor concentrations of 0.066, 0.158, 0.532, 1.038, 1.550, 1.936, 2.461, and 3.195 mmol/L. The concentrations are calculated simply by $c = N_{precursor}/(V_{box}N_A)$, where $N_{precursor}$ is the number of precursors in the simulations, V_{box} is the volume of the simulation boxes, and N_A is Avogadro's number which is needed for unit conversion. The box lengths were 1000, 750, 500, 400, 350, 325, 300, and 275 Å for the respective precursor concentrations. The temperature is maintained constant by using the Anderson thermostat 50 .

Simulations are performed at body temperature (310 K) because the hydrogel's drug transport should take place in the body. The unitless simulation body temperature is taken from our previous paper $(T_{s, body} = 0.58)^{44}$. In our simulations, the temperature is cooled by 0.01 for every 1 million collision from an initial very high temperature of $T_s = 8.0$ until this temperature was achieved. The purpose of using high temperature at the start of the simulation is to spread the precursors uniformly around the simulation box before the actual "reaction" occurs. The annealing schedule was designed to reach body temperature after approximately 500 million collisions; this gives the precursors enough time to spread out evenly over the simulation box.

The percolation probability is used to determine if the network meets the minimum requirements to be a hydrogel or not. We defined an aggregate to be at least two precursors that are connected by a crosslinker. The aggregate is considered a "percolated network" if there is a connected path in the aggregate that spans from one end of the simulation box to the other along a path that connects to its own periodic image in one direction. Although percolation in one direction is a prerequisite for being a gel⁵¹, percolation in three dimensions seems to be necessary for this study in order to have a hydrogel with spaces for storing small molecules (Supplementary Figure 2a). A network percolated in the x and y but not the z directions would be a 2-dimensional slab (Supplementary Figure 2b), and a network percolated in one direction would be an infinitely long string polymer. We introduce the term "percolation criteria" to describe the structures of the aggregates and set the maximum percolation criteria value to be 3; this is the sum of the maximum percolation probabilities in the x, y, and z directions. A percolation criteria of 1, 2, or 3 represents a one-, two-, and three-dimensionally percolated structure. The percolation criteria at a given concentration, \$II\$, is defined as

$$\Pi = < \frac{\sum_{1}^{N} (P_x + P_y + P_z)}{N} >$$

where P_i represents the percolation state of a given configuration that is percolated in the i direction. It is 0 (no percolation) or 1 (percolation). N is the number of configurations observed throughout the simulation, and the observation is taken every one million collisions after the system has reached the equilibrium state. The angle bracket denotes the average of 5 independent simulations at that concentration.

The pore diameter distributions in the percolated network are calculated to quantify its structure. To do this, a random position is selected in the pore and the largest sphere that encompasses that random position is found⁵². The diameter of that sphere is chosen as the diameter of the pore. The simulations for obtaining the pore diameter distributions are conducted for 50 million collisions starting with an already-equilibrated network as an initial configuration. Every 1 million collisions, 2000 random locations are used to measure the pore diameters.

To understand the effect of the pore structure on the migration of molecules in the network, a sphere is inserted into the percolated network and its mean square displacement (MSD) is calculated. The sphere is modeled as a hard sphere, meaning it has no interactions with EOs or with the nucleotides. The interaction distances (sphere diameter) are set to: $\sigma_{sphere-EO} = 0.5*(\sigma_{sphere}-\sigma_{EO})$ and $\sigma_{sphere-DNA}=0.5*(\sigma_{sphere}-\sigma_{DNA})$; the point is just to focus on how network structure affects the MSD. The sizes of sphere inserted into the hydrogel network are 55, 60, 65, 70, and 75 Å. The molar mass of all the spheres is set to be 1.0 g/mol so that the MSD variations become a function of sphere size only⁵³. The MSD was determined from the average of five simulation runs. The starting positions of the spheres were different for each MSD calculation. The directions and magnitudes of the initial velocity of the sphere were different in every

simulation, but the values were chosen so that the kinetic energy of the spheres corresponds to body temperature. The MSD is defined as

$$MSD(\Delta t) = <(r(t + \Delta t) - r(t))^2 >$$

where Δt is the time interval and r(t) is the position of the sphere at time t. The angle bracket denotes an average over time.

Results and discussion

Self-assembly of precursors in presence of crosslinker

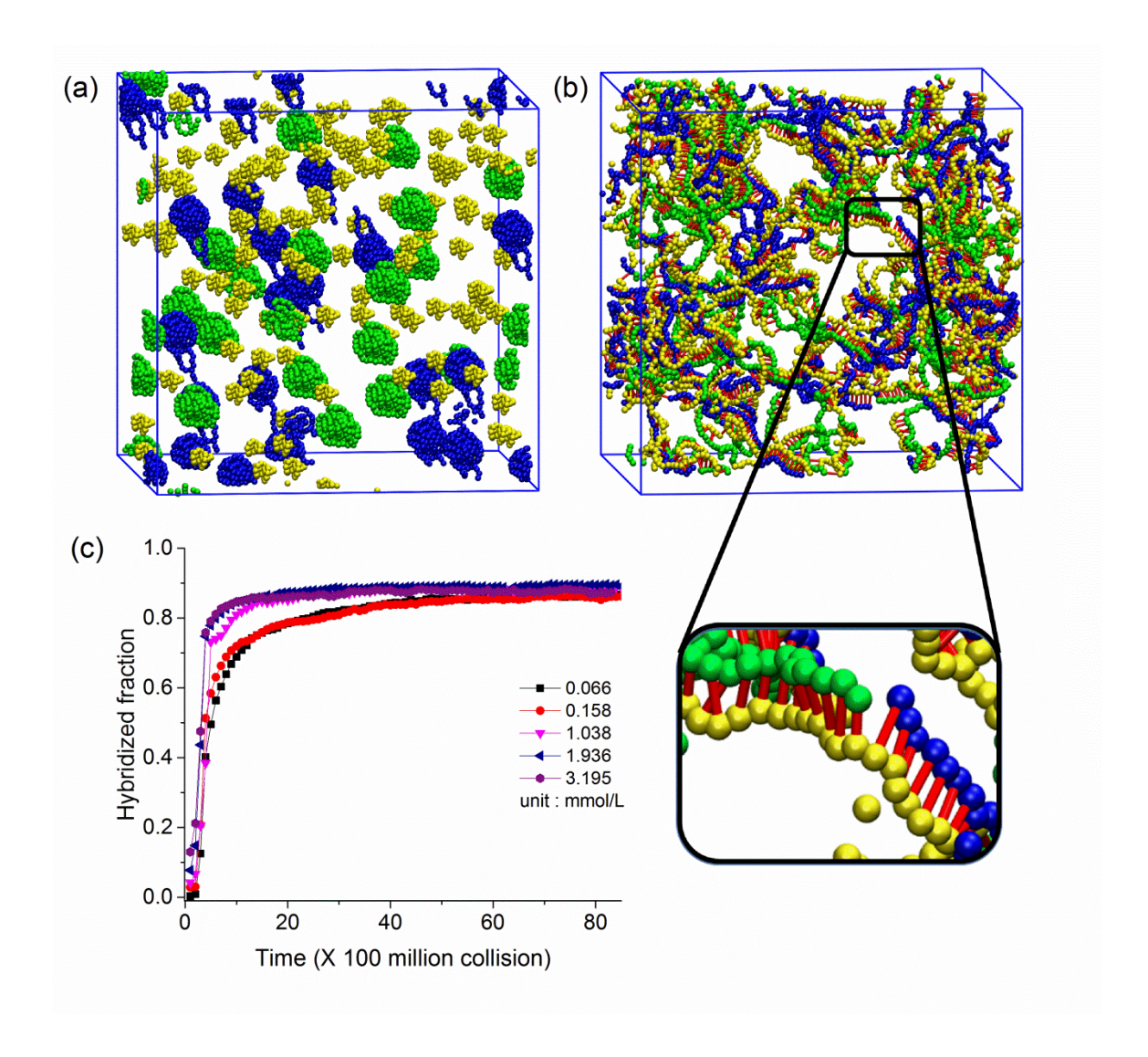


Figure 2. The (a) initial and (b) final snapshots from a simulation containing 6-armed precursors (Blue – Precursor A, green – Precursor B) and crosslinker oligonucleotides (yellow). The inset figure of (b) is an enlarged representation of the hybridization of oligonucleotides; the base-pairing between the CG nucleotide beads is indicated by the red artificial bonds so that the hybridized state can be easily recognized. (c) The hybridized fractions of all oligonucleotides in precursors versus time. Curves of different colors indicate results obtained from different precursor concentrations.

Figures 2 a and b show snapshots of the initial and final configurations for the systems of 6-armed/10 kDa precursors. At the initial configuration, the precursors of A (blue), B (green), and crosslinker strands (yellow) are randomly placed in compact shapes. After 8 billion collisions, Precursor A and B molecules assemble together by hybridizing with the crosslinker strands. The red artificial bonds are used to illustrate the hybridization between precursors and crosslinker strands; chains of connected red bonds which look like ladders indicate complete hybridization. The precursors A and B are evenly distributed throughout the simulation box, and several void spaces which represent the pores of the hydrogel network are observed.

The rate of assembly of the system is quantified by measuring the fraction of precursors and crosslinkers that are hybridized. The hybridized fraction in the equilibrium state is defined as the number of nucleotides in the precursors that are hybridized by the crosslinkers divided by the total number of nucleotides in precursors. Since it is only the number of hybridized nucleotides in precursor that are counted, the actual hybridization fraction is the same regardless of the number of crosslinkers. Note that two crosslinkers can bind to the same arm of a precursor and two arms of a precursor can bind to the same crosslinker in our simulations. However, those binding states are unstable because the nucleotide sequences between the precursor and crosslinkers are not perfectly complementary, so that one crosslinker will eventually occupy only one arm. Figure 2c shows the fraction of total hybridized pairs of 6-armed/2 kDa precursors at various concentrations from 0.066 to 3.195 mmol/L. At the beginning of the simulation, the hybridized fractions are low at every concentration. However, as the simulation proceeds, crosslinkers pair with their complementary oligonucleotide sequences on the precursors and the hybridized fraction increases. The hybridized fractions reach a plateau after about 4 billion collisions; the values for 4-armed and 6-armed precursors are 0.82 - 0.88 and 0.86 - 0.90,

respectively, at all examined concentrations. The degree of saturation is defined as the number of crosslinkers that are hybridized to the precursors divided by the number of crosslinkers needed to fully crosslink the network. Table 2 displays the degree of saturation for the different shaped-precursor systems in the equilibrium state. The degrees of saturation for the 4-armed and 6-armed precursor systems are close to 90%. The 4-armed and 6-armed precursors achieve higher high levels of crosslinking regardless of the molecular weights.

	4-armed	6-armed
2 kDa	89.38	89.19
5 kDa	88.12	89.81
10 kDa	86.38	89.92

Table 2. The saturation degree of precursors with different shapes and molecular weights. Unit: %

Three dimensional percolation; Formation of hydrogel

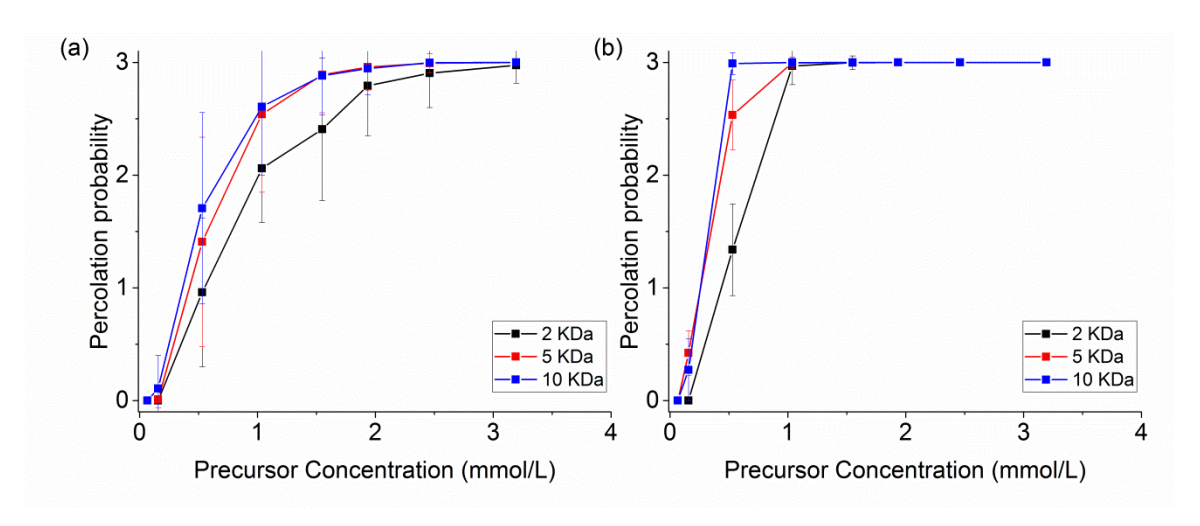


Figure 3. Percolation probability in three dimensions versus the precursor concentrations for (a) 4-armed and (b) 6-armed precursor systems. Black, red, and blue curves in each figure represent precursors with molecular weight of 2, 5, and 10 kDa.

To check whether the clusters that form in the simulations are truly interconnected networks or just disconnected aggregates, the three-dimensional percolation probabilities of the crosslinked structure are calculated as a function of precursor concentration. Recall that unlike the conventional percolation probability which ranges from 0 to 1, the maximum value of the percolation probability in our simulation is 3, which is the sum of the maximum percolation probabilities in x, y, and z directions. Having a value of 3 means that the system has percolated in each of the x, y, and z directions, and that there are void spaces surrounded by network skeleton. The value of percolation probability is determined by averaging the results of five simulations performed at the same concentration. Figures 3 a and b show the percolation probabilities of crosslinked structures formed by 4-armed and 6-armed precursors with molecular weights of 2, 5, and 10 kDa as a function of concentrations. Once again, the length of a single arm for each precursor is: for 4-armed precursor, 11 EOs at 2 kDa, 28 EOs at 5 kDa, and 57 EOs at 10 kDa; for 6-armed precursor, 8 EOs at 2 kDa, 19 EOs at 5 kDa, and 38 EOs at 10 kDa. Note that the heavier precursors have longer PEG lengths. Regardless of the number of arms, precursors with longer lengths percolate at lower concentrations. This implies that larger precursors are better at forming a percolated network than the shorter precursors at the same concentration. The minimum precursor concentration required to form a three-dimensional percolated network is ~3.0 mmol/L for 4-armed precursors. In the case of the 6-armed precursors, three dimensional percolation is first observed at a concentration less than 1.0 mmol/L, relatively low compared to the 4-armed precursors. A noteworthy point is that the degree of percolation for 6-armed precursors increases abruptly at a certain concentration, rather than gently as in networks formed by the 4-armed precursor. In summary, the higher the number

of branches in the precursor and the longer their length, the lower the concentration required to form a three-dimensionally percolated structure.

Pore diameter distribution

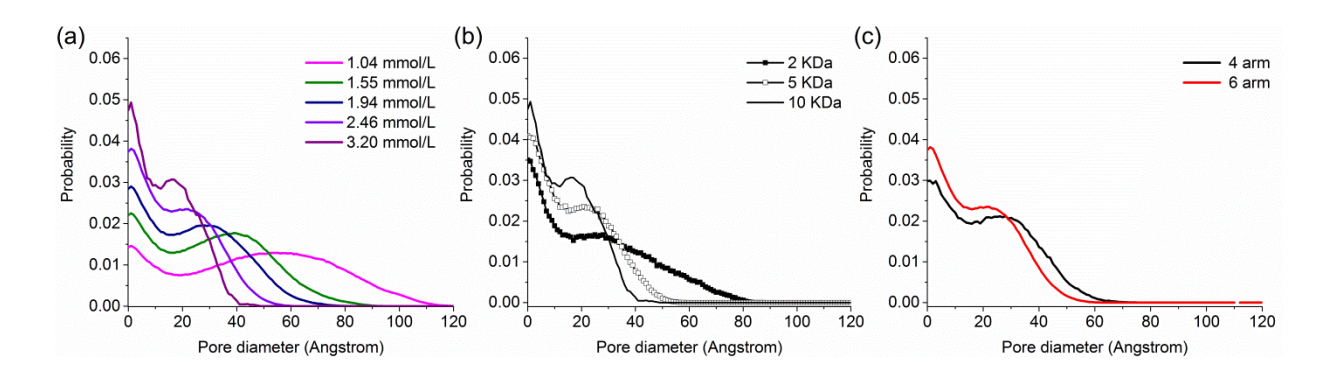


Figure 4. Pore diameter distribution for percolated network of (a) 6-armed/10 kDa at a variety of concentrations, (b) 6-armed/3.20 mmol/L at different molecular weights, and (c) 10 kDa / 2.46 mmol/L with different precursor structures.

The percolated networks contain empty spaces, pores, surrounded by crosslinked precursors; the size of these pores depends on the precursor concentration, molecular weight, and structure. Figure 4 shows the pore diameter distributions of percolated networks. The pore diameter distribution is obtained from a single simulation run because the pore structures formed at fixed precursor concentration in very long runs do not vary much from run to run. This is shown in Supplementary Figure 3, which compares the pore diameter distributions of five different percolated networks (6armed / 10 kDa, precursor concentration 1.55 mmol/L) with different initial configurations. First, high precursor concentration makes the hydrogels more likely to have relatively uniform small-sized pores. Figure 4a displays the pore diameter

distributions for percolated networks of 6-armed /10 kDa precursor at different precursor concentrations. The systems are at higher precursor concentrations than the three dimensional percolation threshold. In all graphs of the pore diameter distribution, very small pores (< 10.0 Å) are commonly found with a high probability. These are formed when several chains cluster together to form bundles, creating innumerable small voids and correspond to the first peak in the figure. A better measure of the topology of the available pore space is the diameter associated with second peak in Figure 4, the local maximum occurring after 10 Å. We will refer to this as the "characteristic diameter". The three-dimensionally percolated networks formed at relatively low precursor concentrations have a broad pore diameter distribution profile. As the precursor concentration increases, the distribution profile gradually narrows and peaks at a higher probability. The characteristic pore diameter decreases as the concentration increases, and ranges from 55 Å at 1.04 mmol/L to 17 Å at 3.20 mmol/L. Supplementary Figure 4 shows the pore distributions at a variety of precursor concentrations for all types of precursors. In all cases, the shapes of the pore diameter distributions are narrow and the characteristic pore diameters are small at high precursor concentrations.

The molecular weight of the PEGs also affects the pore structure of the percolated networks. Figure 4b displays the effect that increasing the precursor's molecular weight has on the pore distribution at a fixed precursor concentration (3.20 mmol/L) and shape (6-armed). The distributions become narrower as the molecular weight increases with characteristic pore diameters of 26, 21, and 17 Å for 2, 5, and 10 kDa molecular weights respectively. Similar results are seen for the rest of the pore distribution curves of percolated network generated by 4-armed and 6-armed precursors (Supplementary Figure 4). Because the volume of the system is constant, the larger the molecular weight of the precursor, the smaller the volume occupied by

the pores, and eventually the pore size decreases. Thus, a negative correlation between the size of the pores and molecular weight of the precursor is observed.

Lastly, precursors with many branches are found to be advantageous for forming uniform porous structures. The influence of the number of branches on the pore size distribution can be seen by comparing the pore diameter distributions for the 4- and 6-armed precursors at fixed precursor molecular weight and concentration. Figure 4c shows the pore distributions of the 4-armed /10 kDa (black) and 6-armed /10 kDa (red) networks at precursor concentration of 2.46 mmol/L. At a fixed concentration and molecular weight, the network formed by 6-armed precursor has a slightly narrower pore diameter distribution than the network formed by the 4-armed precursors. To summarize the three points, relatively narrow pore diameters are established in the three-dimensionally percolated network under the conditions of high precursor concentration, large molecular weight and more branches.

The non-uniformity of the pore structure

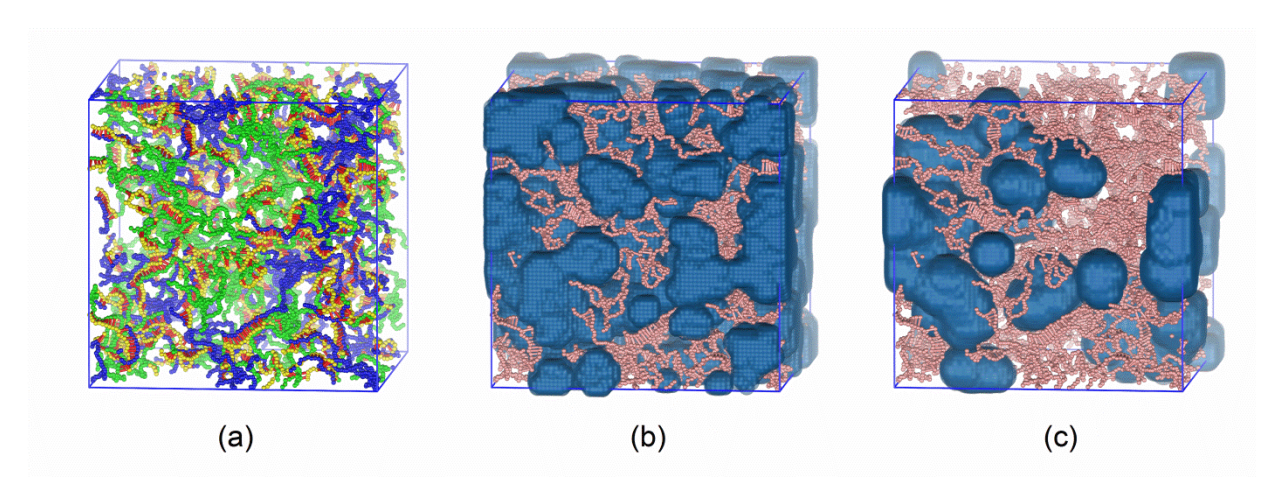


Figure 5. (a) The shape of hydrogel formed by 6-armed/10 kDa precursors at 1.55 mmol/L (blue – Precursor A, green – Precursor B, yellow – crosslinker, and red – artificial bond

representing hybridization). (b) and (c) show the positions of the pores (dark blue) in which molecules of 40.0 and 60.0 Å can move within the hydrogel (pink), respectively.

The non-uniformity of the pore structure limits the movement of molecules located in the percolated networks. Obviously since there is a distribution of pore diameters, there will be pores that molecules of a certain size can reach and pores that they can't reach. Pores of a certain size that are reachable within the hydrogel can be identified by placing virtual spheres of that size in many random locations of the simulation box without overlapping with the hydrogel skeleton (Figure 5a). The shape of a pore within the hydrogel can be visually expressed as a conglomeration of the virtual pores lumped together. The dark blue areas in Figure 5b show the pore structure that small molecules of 40.0 Å diameter can travel through, and those in Figure 5c show the pore structure that large molecules of 60.0 Å diameter can travel through. Comparing the two figures, the volume that molecules of 40.0 Å diameter can travel through is much larger than the volume that molecules of 60.0 Å diameter can travel through. In addition, the space in which small molecules of 40.0 Å can move is connected to its own periodic images in the x, y, and z directions; i.e. the pore structure is in a percolated state. On the other hand, the space in the hydrogel where large molecules of 60.0 Å can move is disconnected. Therefore, relatively small molecules in the hydrogel are allowed to move almost everywhere in the gel matrix, while relatively large molecules have very limited movement because of the hydrogel's non-uniform disconnected pore structure. It follows that there exists a maximum size molecule that can move through the inside of the hydrogel. This is the "throat diameter" of the pore.

The existence of the pore throat

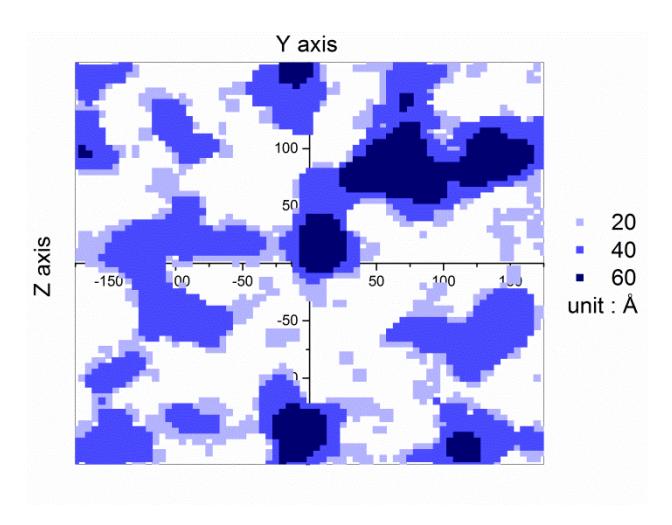


Figure 6. A contour map of pore of hydrogel formed by 6-armed/10 kDa at 1.55 mmol/L at x = -55.0 Å. The areas of the pores that can be reached by different sizes of molecules (20, 40, and 60 Å) are shown in blue colors with different intensities.

The existence of the pore throat diameter is confirmed by observing cross-sectional images of the percolated network. Figure 6 shows the y-z cross-section of percolated network formed by 6-armed /10 kDa with precursor concentration of 1.55 mmol/L at x = -50.0 Å. Different intensities of blue represent pores in which molecules of different diameter from 20.0 to 60.0 Å can travel, respectively. The pore area where a molecule with a diameter of 20.0 Å can travel is distributed throughout the network. As the molecule size increases, the area accessible to molecules of that size decreases gradually; very limited areas are allowed for the motion of molecules with diameters larger than 60.0 Å. Thus, the throat diameter of a pore is determined by investigating the pore connectivity of different diameters.

The pore throat diameter of the hydrogels

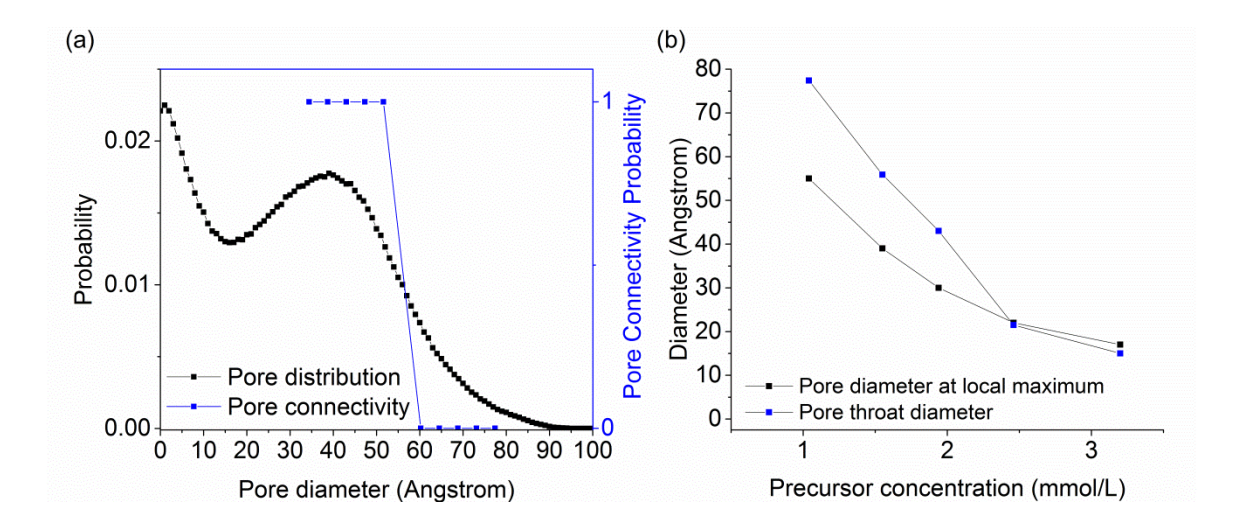


Figure 7. (a) Comparison of pore distribution and connectivity for percolated network by 6-armed/10 kDa at a precursor concentration of 1.55 mmol/L and (b) the characteristic pore diameters and pore connectivity thresholds of percolated network by 6-armed/10 kDa at various precursor concentrations.

The throat diameter of hydrogels decreases as the precursor concentration increases. To determine the throat diameter, virtual beads of 10 different diameters (from 35 to 80 Å in 5 Å intervals) are placed in the pore region of percolated networks. We observe whether the virtual beads are connected in the x, y, and z directions⁵⁴. The connectivity of the virtual beads is verified using the percolation probability concept. The percolation of the virtual beads is quantified in terms of a pore connectivity probability for better understanding. The pore connectivity probability is defined to have a value of 1 if the virtual beads form a chain that percolates across the simulations box regardless of the direction, and 0 otherwise. Unlike our treatment of the hydrogel's percolation in three-dimensions, we do not concern ourselves about the dimensionality of the percolation of a pore. The point is have a connected pore leading to the

outside of the hydrogel; for the purposes of this paper, it is immaterial whether the pore that is formed percolates in only one or two dimensions. However, one suspects that hydrogels with three-dimensionally percolated pores are different in shape than hydrogels with onedimensionally percolated pores, and that the latter will be formed at a much lower precursor concentration than the former. Figure 7a is a graph comparing the pore size distribution (black) and the pore connectivity probability (blue) of a hydrogel prepared using 6-armed/10 kDa at a precursor concentration of 1.55 mmol/L. The characteristic pore size for this case is 39 Å. The pore connectivity probability is constant at 1 up to a pore diameter of 55.90 Å, which means that the pores are percolated. However, the pore connectivity probability drops to zero at 60.20 Å, which means that the pores lose connectivity. From this, we determine that the throat diameter is 55.90 Å which is the largest diameter that maintains pore percolation. The pore throat diameter of the hydrogel can be adjusted to be 16 to 170 Å by varying the molecular weight, the number of branches, and the concentration of the precursors (Supplementary Figure 5). Figure 7b is a graph comparing the characteristic pore diameter and the pore throat diameter for the hydrogel made using the 6-armed/10 kDa precursor at various concentrations. The characteristic pore diameters and the pore throat diameters of the percolated networks decrease as the precursor concentration increases. When the precursor concentration is less than 2.46 mmol/L, the throat diameters are greater than the characteristic pore sizes. However, when the precursor concentration is above 2.46 mmol/L, the throat diameter becomes similar to the characteristic pore diameter suggesting that the connected pores of the hydrogel are like pipes with a constant diameter. In other systems, except 6-armed/10 kDa, the pore throat diameter is always larger than the characteristic diameter at the precursor concentrations considered. Molecules placed inside the hydrogel whose characteristic size is greater than or equal to the throat diameter of the pore will be completely trapped in the hydrogel matrix. Ultimately, to deliver the drug to its destination without loss, a hydrogel with a smaller throat diameter than the size of the drug should be used.

The diffusion of molecules within the network

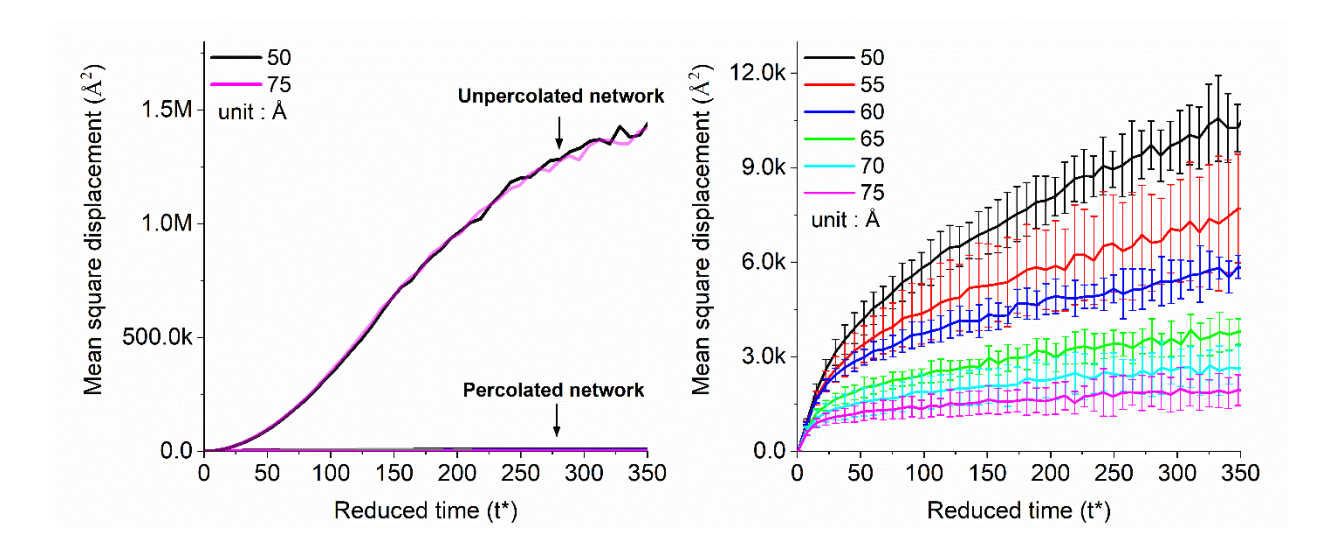


Figure 8. (a) Comparison of the mean square displacement of spheres in an unpercolated network and a three-dimensionally percolated networks. (b) The mean square displacement for each sphere diameter in the three-dimensionally percolated networks. Each color represents the MSD of a molecule with a different diameter.

The movement of small molecules in the percolated networks (hydrogel, 3-dimensionally crosslinked polymer) is more limited than those in the unpercolated networks (separate cluster) when the molecular weight and number of precursor arms are fixed. The unpercolated network was selected only as a comparison to confirm the hydrogel's drug confinement ability. To compare the movement of a molecule inside two different networks, hard spheres of different

sizes are inserted in the networks and the MSD of the spheres are measured. For the measurement of MSD, two networks with 6-armed/10 kDa at 0.01 and 1.55 mmol/L are selected; the first represents an unpercolated network and the second represents a percolated network. The diameters of the spheres inserted in the unpercolated network are 50 and 75 Å, and the diameters of the spheres in the percolated network are 50, 55, 60, 65, 70, and 75 Å which are the size corresponding to the diameter range of ranibizumab (56 Å) and aflibercept (76 Å). Note that the mass of the sphere is constant as 1 g/mol regardless of the diameter in order to maximize the movement of sphere per unit time and avoid mass effects in the MSD. The MSDs of the spheres are measured by inserting them one by one into the network and tracking their positions. Figure 8 shows the results of the MSD measurement of different sized spheres in the two networks. The MSDs of spheres in the unpercolated network are nearly the same for the two sphere diameters (Figure 8a). This is to be expected because the unpercolated network does not have pores surrounded by precursors. However, in the percolated network, the MSDs are significantly reduced compared to those in the unpercolated network regardless of the sphere diameter (Figure 8b). This implies that once three dimensional percolation is established, the movement of the molecule inside the network is constrained by collisions due to the structure of the network. The MSDs of relatively small-sized spheres are high even though the sphere is in the percolated network because they are small enough to move freely without being disturbed. As the sphere diameter increases, the MSDs decrease because the available void space becomes too small.

Conclusion

We describe the results of discontinuous molecular dynamics simulations of the formation and the structural properties of an oligonucleotide-crosslinked PEG based hydrogel. The hydrogel networks are formed by 4- and 6-armed PEG precursors that are covalently functionalized on all ends with oligonucleotides. The crosslinker is a single oligonucleotide whose sequence is complementary to the oligonucleotide conjugated to the precursors. Network formation is achieved by hybridization between the precursor's oligonucleotide moiety and the crosslinker. The formation of a network was investigated in the concentration range from 0.066 to 3.195 mmol/L for each precursor. High levels of crosslinking are achieved for the 4- and 6-armed precursor systems.

When the network is percolated in the x, y, and z directions at a given concentration, it is believed to satisfy the minimum requirements for being a hydrogel. We calculated percolation in three dimensions because it ensures the formation of a hydrogel with cargo space for small molecules. The simulation results show that the likelihood of three-dimensional percolation increases as the precursor concentration increases for all shape precursors. The concentrations needed to form a stable percolated structure are 3.0 and 1.0 mmol / L for the 4- and 6-armed precursors, respectively, regardless of the precursor molecular weights. As the number of branches of the precursor increases, lower precursor concentrations are sufficient to achieve three-dimensional percolation. As the 6-armed precursor has more hybridization sites than 4-armed precursor, crosslinking can be achieved more easily. Thus, 6-armed precursors form stable hydrogel networks at low concentrations.

Next, the pore diameter distributions within the percolated network structures formed by 4- and 6-armed precursors were analyzed. The pore diameter distribution depends on the shape, molecular weight, and concentration of the precursors. In order to form a hydrogel with narrow pore size distributions, a precursor should have many branches and high molecular weight and should be crosslinked at a high concentration. As the pore sizes in DNA-mediated hydrogel are not uniform, the maximum size of a material that could travel freely within the hydrogel should be determined. This maximum size is called the pore throat diameter. The pore throat diameter of the hydrogel is found to be higher than the characteristic diameter (the most frequently observed pore diameter > 10 Å) for most of the investigated structures and precursor concentrations. The reason why the throat diameter is larger than the characteristic diameter is because the smallsized disconnected pores (or separated chambers), which are not associated with connected pores, are included in the pore diameter distribution curve. The hydrogels crosslinked by 6armed/10 kDa precursor at a concentration of 2.46 mmol/L or higher have a pore throat diameter that is similar to the characteristic diameter. The reason that those two diameters are similar at high concentrations is that the sizes of the voids within the pores have become more uniform. Measuring the distribution of connected and disconnected pores would be a new research topic for a deeper understanding of the structure of hydrogels. When the hydrogel is used as a drug delivery vehicle for loading molecules that are smaller than pore throat diameter, immersion of the hydrogel in a liquid to load drug molecules into the hydrogel by equilibrium partitioning would work. However, at the same time, it would be possible for the molecules to escape from the hydrogel before it reaches the target site.

Lastly, the drug carrying ability of the percolated network (hydrogel) was verified by analyzing the diffusion of spheres in the networks. Spheres of various size diameters (55, 60, 65,

70, and 75 Å) were placed in percolated networks formed by 6-armed precursors at 1.55 mmol/L precursor concentration, and the MSD of the beads was calculated. As a control, the MSD of the same sized beads in a network formed at 0.16 mmol/L, an unpercolated network, was measured. The MSDs of the various sized beads in the unpercolated network with 0.16 mmol/L are similar because the void space is larger than the size of the inserted beads. On the other hand, the MSDs of all size beads in the percolated network (1.55 mmol/L) decrease because the movement of beads is reduced by colliding with the scaffolds of the networks. As the bead diameter increases, the MSD gradually decreases because the pore space becomes too small for the beads to move in the hydrogel network. When the size of the bead is greater than the pore throat diameter, the MSD is relatively independent of the bead size, indicating that the material is entrapped. For example, ranibizumab (a drug for macular degeneration with hydrodynamic diameter: 55.2 Å) can be carried by the hydrogel formed with 6-armed/10 kDa at the concentration of 1.94 mmol/L since its pore throat diameter is 43.0 Å.

The main conclusions that can be drawn from this simulation study of oligoncuelotide-crosslinked hydrogels are the following: 1) The required concentration for the formation of the hydrogels by various precursor shapes is predicted to be; 3.0 mmol/L for 4-armed precursors and 1.0 mmol/L for 6-armed precursors. 2) The structure of the formed hydrogel can be understood through the pore diameter distribution and pore connectivity analysis; pore size distributions indicate the extent to which the pore structures are non-uniform and the pore connectivity probability allows determination of the pore throat diameter. 3) The drug-carrying ability of the hydrogel can be analyzed by measuring the MSD of small molecules in the hydrogel; percolated networks show lower MSDs than unpercolated networks. 4) The size of drugs should be larger than the pore throat diameter to deliver them without leaking. There results could be used to

design DNA crosslinked hydrogels for drug delivery application by adjusting the structure and concentration of the precursors to control porosities.

In next stage of this project, we will develop a model of a target molecule (adenosine) that triggers the DNA crosslinks to unhybridize, and consequently the hydrogel to degrade and release drugs, by inclusion of a specific oligonucleotide (aptamer) sequence as part of the crosslinker. The crosslinker will be extended to include an aptamer sequence to react with the target. Assuming a situation where the hydrogel meets the target molecule, the adenosine will be introduced into the hydrogel network. The hydrogel network generated by the simulation will be used as an initial configuration to observe interaction with molecular targets.

Although our CG simulations provide molecular-level understanding of the formation and drug carrying ability of oligonucleotide-crosslinked hydrogels, the model has several limitations. First, the drug molecule is designed not to have any interactions with the hydrogel components. In reality, drug molecules would interact with the PEG or the nucleotide via electrostatic interactions, hydrophobic interactions and/or hydrogen bonding, affecting the movement of drug molecules. In future work, we will go beyond our current description of the geometric aspect of drug-pore size and focus more on the chemical nature of the drug molecules. Several specific cancer drug molecules will be considered. CG parameters (well-depth, well-width, and number of wells) for the drug-PEG, drug-nucleotide and drug-drug interactions will be determined from atomistic simulations. This would give us a fuller picture of how the chemical nature of the drug molecules affects their role as guest molecules in the hydrogel host scaffold. Second, water is treated implicitly in our simulation and the absence of hydrodynamics would have distorted the structure of the hydrogel somewhat differently from the actual one. In

addition, because our implicit solvent model assumes that the solvent is water, it is not possible to predict the behaviors of drug molecules that are immiscible in water. Third, as our drug model is a simple hard sphere, it is not sufficient to distinguish between the diffusion of hydrophilic and hydrophobic drugs in the hydrogel. As PEG and nucleotides are both hydrophilic, we expect that the interaction between hydrophilic drug molecules and the hydrogel would be stronger than the interaction between hydrophobic drug molecules and the hydrogel. The movement or diffusion of the hydrophilic molecules in the hydrogel should be slower than that of the hydrophobic molecules if the two molecules' diameters are the same. Finally, in order to predict conditions under which a hydrogel would actually form, we need to analyze not only the network percolation but also its mechanical properties such as the modulus.

Acknowledgement

This work was supported by the National Institutes of Health (EB006006), the NSF's Research Triangle MRSEC on Programmable Soft Matter, DMR-1121107 and CBET 1512059, and the NSF Partnership for Research and Education in Materials (PREM), DMR-1205670.

Supporting Information

Comparison of the RDFs of the atomistic and CG EO models, the projection views of 3dimensionally and 2-dimensionally percolated networks with periodic duplications, pore diameter distributions of five independent percolated networks formed by different initial configuration and velocity at the same precursor concentration, pore diameter distributions of networks and pore throat diameters of percolated network formed by different precursor structures.

Reference

- 1. Mellati, A.; Dai, S.; Bi, J.; Jin, B.; Zhang, H., A biodegradable thermosensitive hydrogel with tuneable properties for mimicking three-dimensional microenvironments of stem cells. *RSC Advances* **2014**, *4* (109), 63951-63961.
- 2. Ahmed, E. M., Hydrogel: Preparation, characterization, and applications: A review. *Journal of Advanced Research* **2015**, *6* (2), 105-121.
- 3. Seliktar, D., Designing Cell-Compatible Hydrogels for Biomedical Applications. *Science* **2012**, *336* (6085), 1124-1128.
- 4. Appel, E. A.; Loh, X. J.; Jones, S. T.; Biedermann, F.; Dreiss, C. A.; Scherman, O. A., Ultrahigh-Water-Content Supramolecular Hydrogels Exhibiting Multistimuli Responsiveness. *Journal of the American Chemical Society* **2012**, *134* (28), 11767-11773.
- 5. Naahidi, S.; Jafari, M.; Logan, M.; Wang, Y.; Yuan, Y.; Bae, H.; Dixon, B.; Chen, P., Biocompatibility of hydrogel-based scaffolds for tissue engineering applications. *Biotechnology Advances* **2017**, *35* (5), 530-544.
- 6. Jacob, J. T., Biocompatibility in the Development of Silicone-Hydrogel Lenses. *Eye & Contact Lens-Science and Clinical Practice* **2013**, *39* (1), 13-19.
- 7. Nicolson, P. C.; Vogt, J., Soft contact lens polymers: an evolution. *Biomaterials* **2001**, *22* (24), 3273-3283.
- 8. Slaughter, B. V.; Khurshid, S. S.; Fisher, O. Z.; Khademhosseini, A.; Peppas, N. A., Hydrogels in Regenerative Medicine. *Advanced Materials* **2009**, *21* (32-33), 3307-3329.
- 9. Grainger, D. W., WOUND HEALING Enzymatically crosslinked scaffolds. *Nature Materials* **2015**, *14* (7), 662-664.
- 10. Camci-Unal, G.; Annabi, N.; Dokmeci, M. R.; Liao, R.; Khademhosseini, A., Hydrogels for cardiac tissue engineering. *Npg Asia Materials* **2014**, *6*, e99.
- 11. Hubbell, J. A., BIOMATERIALS IN TISSUE ENGINEERING. *Bio-Technology* **1995**, *13* (6), 565-576.
- 12. Censi, R.; Di Martino, P.; Vermonden, T.; Hennink, W. E., Hydrogels for protein delivery in tissue engineering. *Journal of Controlled Release* **2012**, *161* (2), 680-692.
- 13. Nicodemus, G. D.; Bryant, S. J., Cell encapsulation in biodegradable hydrogels for tissue engineering applications. *Tissue Engineering Part B-Reviews* **2008**, *14* (2), 149-165.
- 14. Skilling, K. J.; Citossi, F.; Bradshaw, T. D.; Ashford, M.; Kellam, B.; Marlow, M., Insights into low molecular mass organic gelators: a focus on drug delivery and tissue engineering applications. *Soft Matter* **2014**, *10* (2), 237-256.
- 15. Peppas, N. A.; Van Blarcom, D. S., Hydrogel-based biosensors and sensing devices for drug delivery. *Journal of Controlled Release* **2016**, *240*, 142-150.
- 16. Hoare, T. R.; Kohane, D. S., Hydrogels in drug delivery: Progress and challenges. *Polymer* **2008**, *49* (8), 1993-2007.

- 17. Raemdonck, K.; Demeester, J.; De Smedt, S., Advanced nanogel engineering for drug delivery. *Soft Matter* **2009**, *5* (4), 707-715.
- 18. Li, J.; Zheng, C.; Cansiz, S.; Wu, C. C.; Xu, J. H.; Cui, C.; Liu, Y.; Hou, W. J.; Wang, Y. Y.; Zhang, L. Q.; Teng, I. T.; Yang, H. H.; Tan, W. H., Self-assembly of DNA Nanohydrogels with Controllable Size and Stimuli-Responsive Property for Targeted Gene Regulation Therapy. *Journal of the American Chemical Society* **2015**, *137* (4), 1412-1415.
- 19. Lin, C. C.; Metters, A. T., Hydrogels in controlled release formulations: Network design and mathematical modeling. *Advanced Drug Delivery Reviews* **2006**, *58* (12-13), 1379-1408.
- 20. Parker, J.; Mitrousis, N.; Shoichet, M. S., Hydrogel for Simultaneous Tunable Growth Factor Delivery and Enhanced Viability of Encapsulated Cells in Vitro. *Biomacromolecules* **2016**, *17* (2), 476-484.
- 21. El-Sherbiny, I.; Khalil, I.; Ali, I.; Yacoub, M., Updates on smart polymeric carrier systems for protein delivery. *Drug Development and Industrial Pharmacy* **2017**, *43* (10), 1567-1583.
- 22. Li, J. Y.; Mooney, D. J., Designing hydrogels for controlled drug delivery. *Nature Reviews Materials* **2016**, *1* (12).
- 23. Li, X.; Watanabe, N.; Sakai, T.; Shibayama, M., Probe Diffusion of Sol-Gel Transition in an Isorefractive Polymer Solution. *Macromolecules* **2017**, *50* (7), 2916-2922.
- 24. Shibayama, M.; Isaka, Y.; Shiwa, Y., Dynamics of probe particles in polymer solutions and gels. *Macromolecules* **1999**, *32* (21), 7086-7092.
- 25. Jiang, L.; Granick, S., Real-Space, in Situ Maps of Hydrogel Pores. *ACS Nano* **2017,** *11* (1), 204-212.
- 26. Masaro, L.; Zhu, X. X., Physical models of diffusion for polymer solutions, gels and solids. *Progress in Polymer Science* **1999**, *24* (5), 731-775.
- 27. Kamerlin, N.; Elvingson, C., Tracer diffusion in a polymer gel: simulations of static and dynamic 3D networks using spherical boundary conditions. *Journal of Physics-Condensed Matter* **2016**, *28* (47).
- 28. Johansson, L.; Elvingson, C.; Loefroth, J. E., Diffusion and interaction in gels and solutions. 3. Theoretical results on the obstruction effect. *Macromolecules* **1991**, *24* (22), 6024-6029.
- 29. Netz, P. A.; Dorfmüller, T., Computer simulation studies of diffusion in gels: Model structures. *The Journal of Chemical Physics* **1997**, *107* (21), 9221-9233.
- 30. Masoud, H.; Alexeev, A., Permeability and Diffusion through Mechanically Deformed Random Polymer Networks. *Macromolecules* **2010**, *43* (23), 10117-10122.
- 31. Amsden, B., Solute diffusion within hydrogels. Mechanisms and models. *Macromolecules* **1998**, *31* (23), 8382-8395.
- 32. Rouquerol, J.; Avnir, D.; Fairbridge, C. W.; Everett, D. H.; Haynes, J. H.; Pernicone, N.; Ramsay, J. D. F.; Sing, K. S. W.; Unger, K. K., RECOMMENDATIONS FOR THE CHARACTERIZATION OF POROUS SOLIDS. *Pure and Applied Chemistry* **1994**, *66* (8), 1739-1758.
- 33. Peppas, N. A.; Hilt, J. Z.; Khademhosseini, A.; Langer, R., Hydrogels in biology and medicine: From molecular principles to bionanotechnology. *Advanced Materials* **2006**, *18* (11), 1345-1360.
- 34. Kubo, T.; Arimura, S.; Tominaga, Y.; Naito, T.; Hosoya, K.; Otsuka, K., Molecularly Imprinted Polymers for Selective Adsorption of Lysozyme and Cytochrome c Using a PEG-Based Hydrogel: Selective Recognition for Different Conformations Due to pH Conditions. *Macromolecules* **2015**, *48* (12), 4081-4087.
- 35. Kim, J.; Kong, Y. P.; Niedzielski, S. M.; Singh, R. K.; Putnam, A. J.; Shikanov, A., Characterization of the crosslinking kinetics of multi-arm poly(ethylene glycol) hydrogels formed via Michael-type addition. *Soft Matter* **2016**, *12* (7), 2076-2085.
- 36. Tan, H. P.; DeFail, A. J.; Rubin, J. P.; Chu, C. R.; Marra, K. G., Novel multiarm PEG-based hydrogels for tissue engineering. *Journal of Biomedical Materials Research Part A* **2010**, *92A* (3), 979-987.

- 37. Sakai, T.; Matsunaga, T.; Yamamoto, Y.; Ito, C.; Yoshida, R.; Suzuki, S.; Sasaki, N.; Shibayama, M.; Chung, U. I., Design and fabrication of a high-strength hydrogel with ideally homogeneous network structure from tetrahedron-like macromonomers. *Macromolecules* **2008**, *41* (14), 5379-5384.
- 38. Apostolides, D. E.; Sakai, T.; Patrickios, C. S., Dynamic Covalent Star Poly(ethylene glycol) Model Hydrogels: A New Platform for Mechanically Robust, Multifunctional Materials. *Macromolecules* **2017**, *50* (5), 2155-2164.
- 39. Sakai, T., Gelation mechanism and mechanical properties of Tetra-PEG gel. *Reactive and Functional Polymers* **2013**, *73* (7), 898-903.
- 40. Kamata, H.; Akagi, Y.; Kayasuga-Kariya, Y.; Chung, U.-i.; Sakai, T., "Nonswellable" Hydrogel Without Mechanical Hysteresis. *Science* **2014**, *343* (6173), 873-875.
- 41. Yang, H. H.; Liu, H. P.; Kang, H. Z.; Tan, W. H., Engineering target-responsive hydrogels based on aptamer Target interactions. *Journal of the American Chemical Society* **2008**, *130* (20), 6320-+.
- 42. Barker, K.; Rastogi, S. K.; Dominguez, J.; Cantu, T.; Brittain, W.; Irvin, J.; Betancourt, T., Biodegradable DNA-enabled poly(ethylene glycol) hydrogels prepared by copper-free click chemistry. *Journal of Biomaterials Science-Polymer Edition* **2016**, *27* (1), 22-39.
- 43. Yongzheng, X.; Enjun, C.; Yang, Y.; Ping, C.; Tao, Z.; Yawei, S.; Zhongqiang, Y.; Dongsheng, L., Self-Assembled DNA Hydrogels with Designable Thermal and Enzymatic Responsiveness. *Advanced Materials* **2011**, *23* (9), 1117-1121.
- 44. Wang, K. W.; Barker, K.; Benner, S.; Betancourt, T.; Hall, C. K., Development of a simple coarse-grained DNA model for analysis of oligonucleotide complex formation. *Molecular Simulation* **2018**, 1-12.
- 45. Hirvonen, L. M.; Fruhwirth, G. O.; Srikantha, N.; Barber, M. J.; Neffendorf, J. E.; Suhling, K.; Jackson, T. L., Hydrodynamic Radii of Ranibizumab, Aflibercept and Bevacizumab Measured by Time-Resolved Phosphorescence Anisotropy. *Pharm Res* **2016**, *33* (8), 2025-2032.
- 46. Espinosa-de la Garza, C. E.; Miranda-Hernández, M. P.; Acosta-Flores, L.; Pérez, N. O.; Flores-Ortiz, L. F.; Medina-Rivero, E., Analysis of therapeutic proteins and peptides using multiangle light scattering coupled to ultra high performance liquid chromatography. *Journal of Separation Science* **2015**, 38 (9), 1537-1543.
- 47. Rapaport, D. C., Molecular dynamics study of a polymer chain in solution. *The Journal of Chemical Physics* **1979**, *71* (8), 3299-3303.
- 48. Bruns, W.; Bansal, R., Molecular dynamics study of a single polymer chain in solution. *The Journal of Chemical Physics* **1981**, *74* (3), 2064-2072.
- 49. Hezaveh, S.; Samanta, S.; Milano, G.; Roccatano, D., Structure and dynamics of 1,2-dimethoxyethane and 1,2-dimethoxypropane in aqueous and non-aqueous solutions: A molecular dynamics study. *The Journal of Chemical Physics* **2011**, *135* (16), 164501.
- 50. Andersen, H. C., Molecular dynamics simulations at constant pressure and/or temperature. *The Journal of Chemical Physics* **1980**, *72* (4), 2384-2393.
- 51. Emanuela, Z., Colloidal gels: equilibrium and non-equilibrium routes. *Journal of Physics: Condensed Matter* **2007**, *19* (32), 323101.
- 52. Bhattacharya, S.; Gubbins, K. E., Fast Method for Computing Pore Size Distributions of Model Materials. *Langmuir* **2006**, *22* (18), 7726-7731.
- 53. Benner, S. W.; Hall, C. K., Effect of Monomer Sequence and Degree of Acetylation on the Self-Assembly and Porosity of Chitosan Networks in Solution. *Macromolecules* **2016**, *49* (14), 5281-5290.
- 54. Wang, K. W.; Hall, C. K., Characterizing the pore throat diameter of a hydrogel using percolation theory. *Manuscript in preparation* **2018**.